Chiral Porphyrin-SiO_2 Nano Helices-based Sensors for Vapor Enantiomers Recognition

Ilaria Di Filippo[1], Zakaria Anfar[2], Gabriele Magna[1,], Piyanan Pranee[2], Donato Monti[3], Manuela Stefanelli[1], Reiko Oda[2], Corrado Di Natale[4], Roberto Paolesse[1]*

[1]Department of Chemical Science and Technologies, University of Rome Tor Vergata, via della Ricerca Scientifica 1, 00133 Rome, Italy

[2]Univ. Bordeaux, CNRS, Bordeaux INP, CBMN, UMR 5248, 33600 Pessac, France;

[3]Department of Chemistry, Sapienza, University of Rome, Piazzale Aldo Moro 5, 00185 Rome, Italy

[4]Department of Electronic Engineering, University of Rome Tor Vergata, via del Politecnico 1, 00133 Rome, Italy

Supporting information

1. Materials

All reagent grade solvents and chemicals for the synthesis were received from Sigma Aldrich and used without further purification.

1.1 Preparation of chiral nanostructures based on silica Nano helices

1.1.1 Synthesis of 16-2-16 gemini tartrate

The synthesis of 16-2-16 gemini tartrate was performed as previously reported, starting from N, N, N′, N′-tetramethylethylenediamine and 1-bromohexadecane then exchanging the bromide counterion to acetate using silver acetate then to enantiopure tartrate using tartaric acid [2]. The chemical structure of the synthesized 16-2-16 gemini tartrate was confirmed by Fourier transform infrared spectroscopy (FTIR) and proton nuclear magnetic resonance spectroscopy (^{1}H-NMR) measurements[2].

1.1.2 Synthesis of the hybrid silica nano helices (RHH/LHH hybrid)

The powder of 16-2-16 gemini tartrate was dissolved into water at 70 °C (1 mM) and then aged for four days at 20 °C. Typical used quantities are 20 mg of powder for 28 mL of ultrapure water[3]. Then, 16−2−16 L- or D-tartrate self-assemblies are used as templates to prepare silica nanostructures like helix through a sol-gel transcription procedure. In a typical preparation, 0.5 mL of tetraethoxysilane (TEOS) was added to 10 mL of 10^{-4} M aqueous solution of D- or L-tartaric acid and prehydrolyzed at 20 °C by stirring on the roller mixer for 7 h. Then, 5 mL of pre hydrolyzed TEOS was mixed with 5 mL of organic gels and stirred at 20 °C in a roller mixer overnight. Once the transcription was completed, the mixture was washed thoroughly by centrifugation in Mill Q (4 °C) five times.

1.1.3 Synthesis of the inorganic silica nano helices (RHH/LHH inorg)

The 16−2−16 L- or D-tartrate templates were removed by washing with 10 mL methanol at 60 °C (five times), then by ethanol and isopropanol (5mL/5mL) under sonication (twice times) and finally absolute ethanol (three times) using centrifugation at 3893 g for 10 min alternately[4]. The prepared inorganic silica Helix concentration was adjusted to 1 mg/mL (5 mL). Finally, the suspensions are made more homogeneous by breaking helices using tip sonication and then kept in ethanol at room temperature for further use.

1.1.4 Synthesis of the amine inorganic silica nano helices (RHH/LHH)

Inorganic silica Nano helices were functionalized with (3-aminopropyl)triethoxysilane (APTES)[5]. Therefore, 20 µL of APTES was added per 1 mg/mL of silica Nano helices in absolute ethanol. Then, the mixture was kept in an oil bath at 80 °C overnight. This procedure was repeated once to improve the grafting density of amines. The modified silica nanostructure was washed three times with absolute ethanol for further use.

1.1.5 Preparation of porphyrin functionalized silica nano helices

Chiral inorganic silica-NH_2 nanohelices reacted with the activated carboxylic acid groups of ZnpCTPP, (L)ZnP, and (D)ZnP. For this purpose, in a 5 mL clean round bottom balloon, 1 mg of porphyrin molecules in dry DMF (1 mL) was added and kept at 0°C (by using glass) for 5 min. Then, 1 mg of 1-Ethyl-3-(3-dimethylaminopropyl)carbodiimide (EDC), 1 mg of 1-Hydroxybenzotriazole hydrate (HOBt) and 5 µL N-methylmorpholine were added to this solution for 1 hour at 0°C under N_2. After 1 hour of stirring,1 mL of RHH or LHH (1mg/mL) in dry methanol was added. The mixture was kept at 25 °C for 48h under N_2. Then, the suspension was sonicated for 5 min, centrifugated using ethanol (20000 tr/min for 20 min), and the supernatant was removed. This procedure removes the unreacted or non-grafted porphyrins until the supernatant appears colorless.

2. QMB measurements

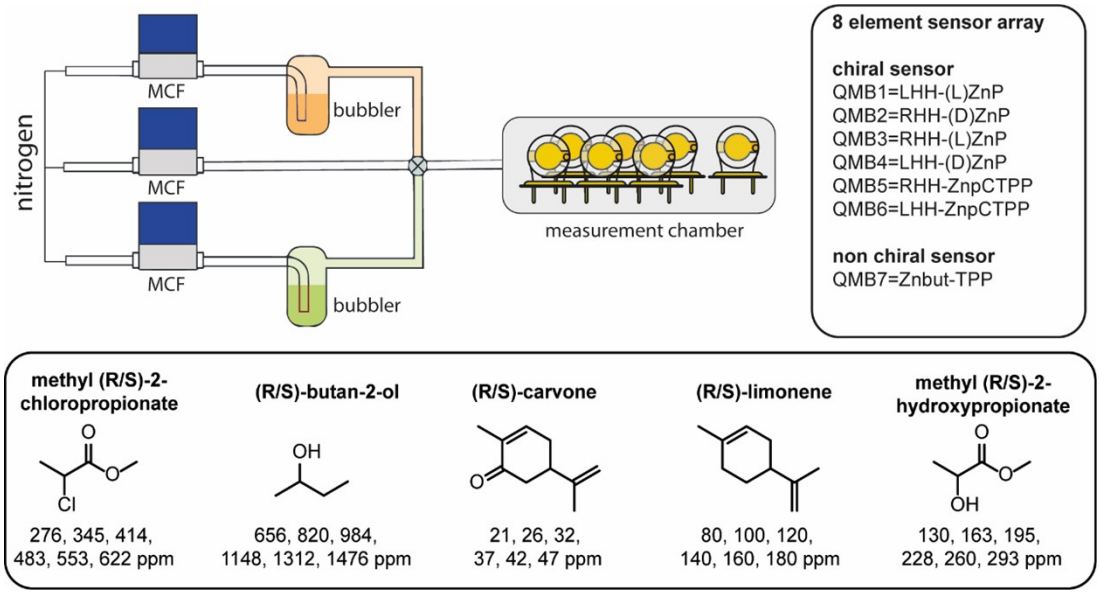

Figure S1. Sensor array setup used for gas measurements. The sensor array includes six chiral sensors and one nonchiral sensors used as references.

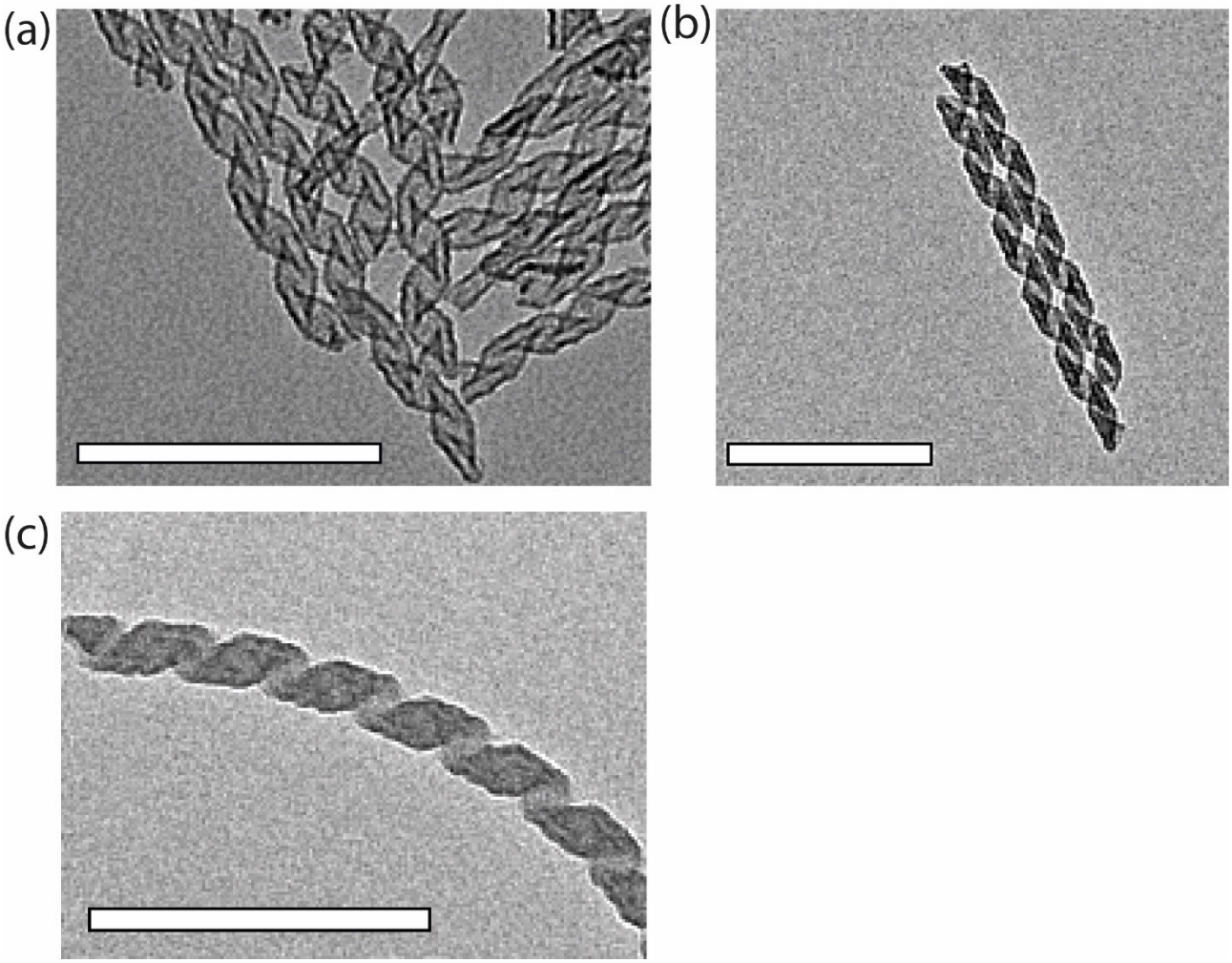

Figure S1. TEM images of A) LHH-inorg, B) LHH, and C) LHH-ZnpCTPP. Scalebars correspond to 200 nm

Table S1. QMB deposition details.

Position	Sensing material	Initial frequency (Hz)	Final frequency (Hz)	ΔF (Hz)	Δm deposited (μg)
QMB1	LHH-(L)ZnP	20000629	19959286	41343	5.74
QMB2	RHH-(D)ZnP	20015292	19972000	43292	6.01
QMB3	RHH-(L)ZnP	20004291	19960816	43475	6.04
QMB4	LHH-(D)ZnP	19981603	19940936	40667	5.65
QMB5	RHH-ZnpCTPP	20041932	20001602	40330	5.60
QMB6	LHH-ZnpCTPP	19975889	19935052	40837	5.67
QMB7	Znbut-TPP	20000675	19967685	32990	4.58

3. Spectroscopic characterization

3.1 Fourier Transform Infrared Spectroscopy (FTIR)

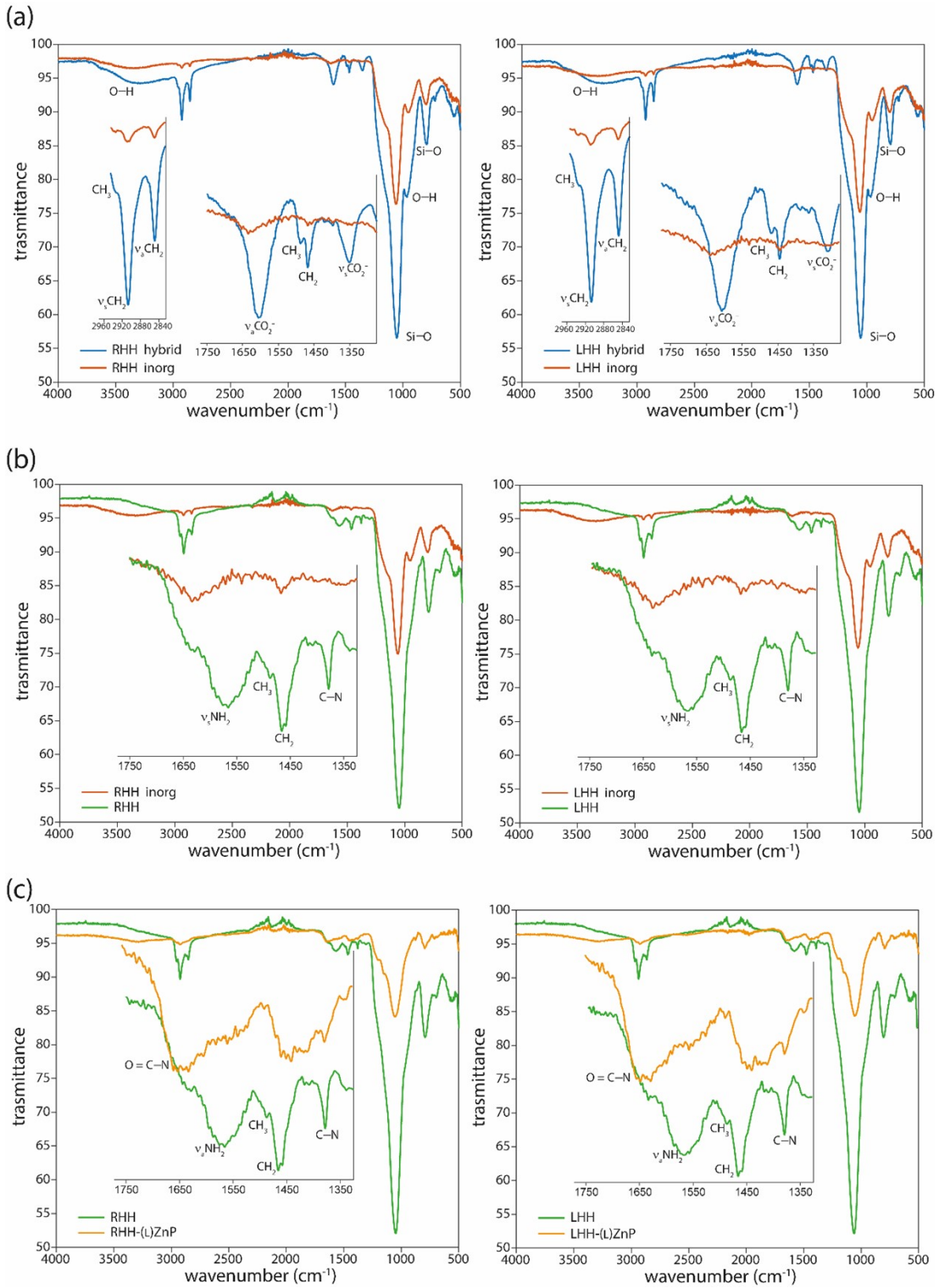

Figure S3. Comparison of FTIR spectra of A) RHH-hybrid and LHH-hybrid (blue lines) with RHH-inorg and LHH-inorg materials (red lines); B) RHH-inorg and LHH-inorg (red lines) with RHH and LHH (green lines); C) RHH and LHH (green lines) with RHH-(L)ZnP and LHH-(L)ZnP (yellow lines).

Table S2. List of all absorption IR bands and corresponding vibrational modes.

group	wavenumber (cm^{-1})	group	wavenumber (cm^{-1})
Si-O internal asymmetric stretching	797	CH_3 bending	1500
Si-O external asymmetric stretching	1058	CH_3 stretching	2957
O-H stretching	3312	CH_2 asymmetric stretching	2853
O-H bending	963	CH_2 symmetric stretching	2923
CO_2 asymmetric stretching	1601	NH_2 symmetric stretching	1561
CO_2 symmetric stretching	1351	C-N	1379
CH_2 bending	1469	O=C-N	1649

3.2 UV - Vis and Circular Dichroism

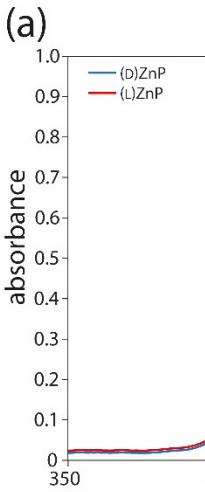

Figure S4. A) UV-Vis and B) CD spectra of ethanol solutions of (D)ZnP (blue line) and (L)ZnP (red line)

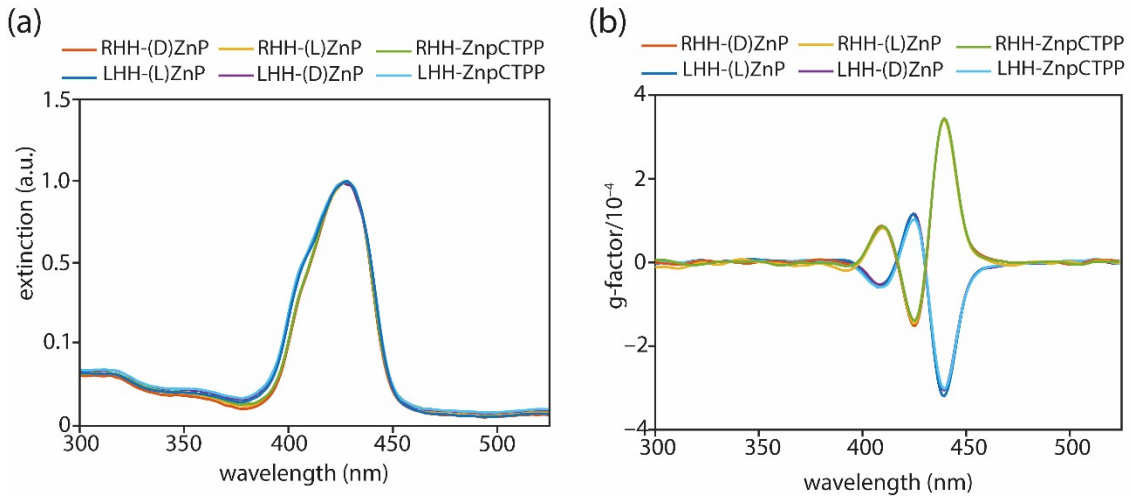

Figure S5. A) UV-Vis and B) g-factor spectra of porphyrins functionalized chiral silica nano helices in ethanol.

Table S3. g-factor values for precursors and prepared systems in corresponding wavelength and solvents

	g-factor	
	Suspension ($x10^{-4}$) (λ=440 nm)	Solid film on glass ($x10^{-4}$) (λ=447 nm)
LHH-(L)ZnP	-3.3	-11
RHH-(D)ZnP	+3.4	+9.1
RHH-(L)ZnP	+3.4	+8.5
LHH-(D)ZnP	-3.1	-9.6
RHH-ZnpCTPP	+3.4	+8.8
LHH-ZnpCTPP	-3.0	-10

4. Sensor measurements

4.1 Data responses

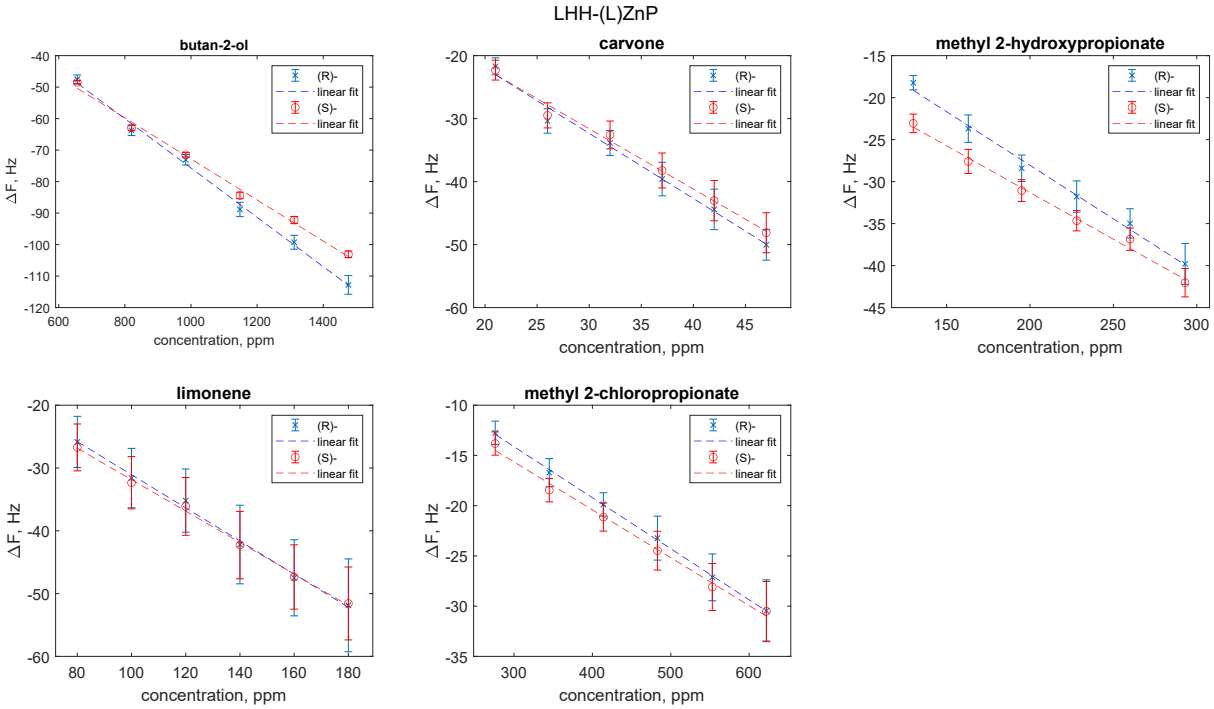

Figure S6. Characteristic curves of LHH-(L)ZnP sensor to the five enantiomer pairs.

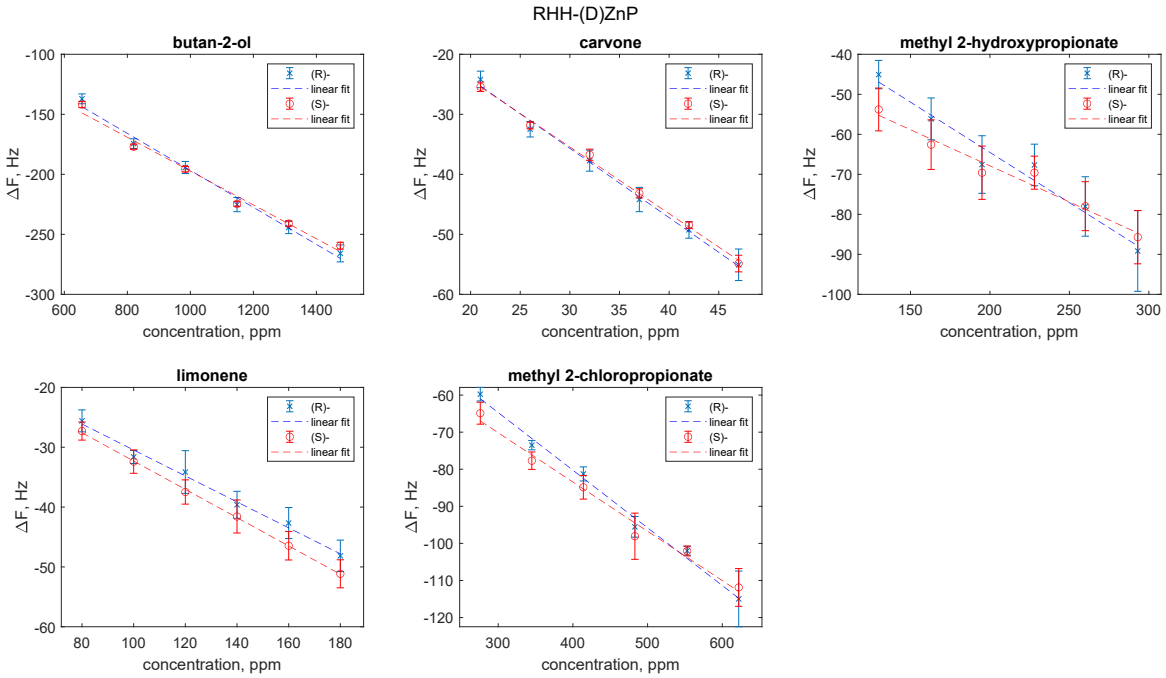

Figure S7. Characteristic curves of RHH-(D)ZnP sensor to the five enantiomer pairs.

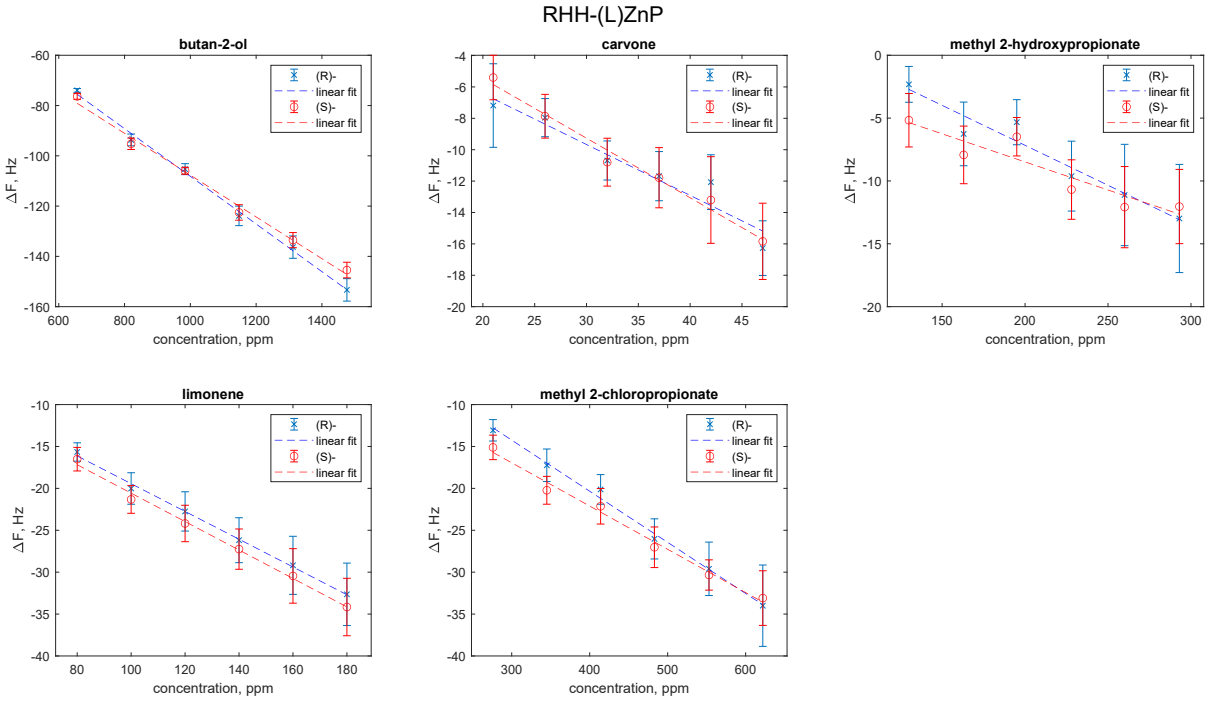

Figure S8. Characteristic curves of RHH-(L)ZnP sensor to the five enantiomer pairs.

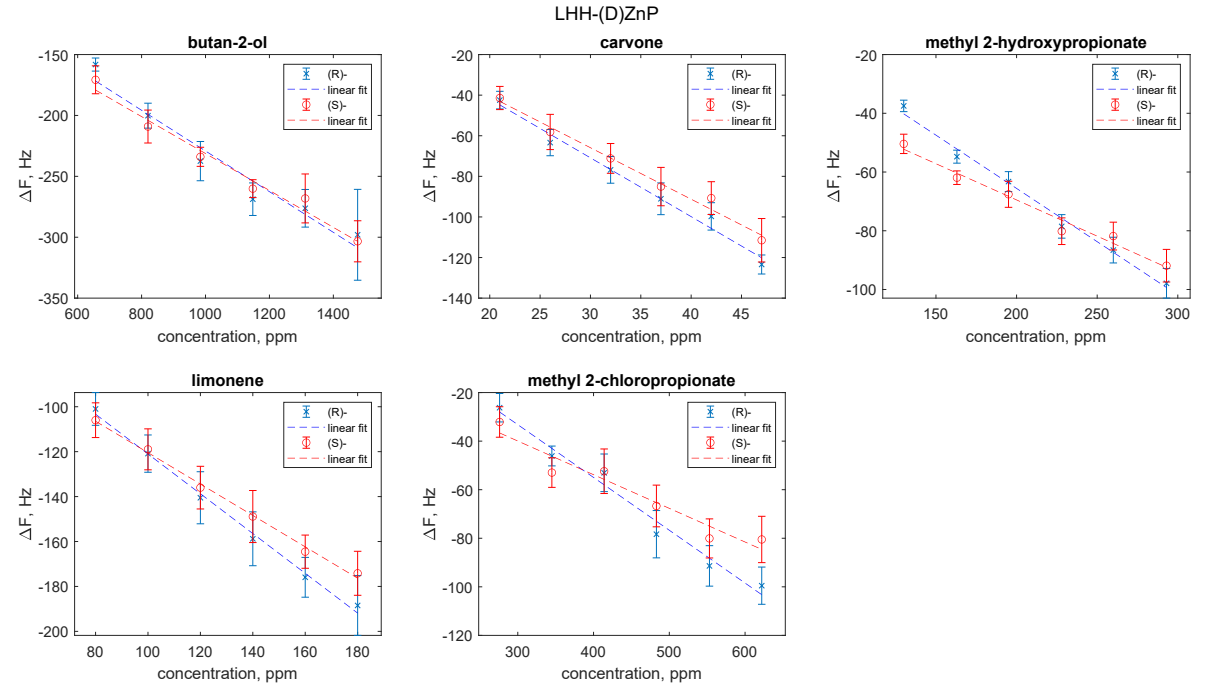

Figure S9. Characteristic curves of LHH-(D)ZnP sensor to the five enantiomer pairs.

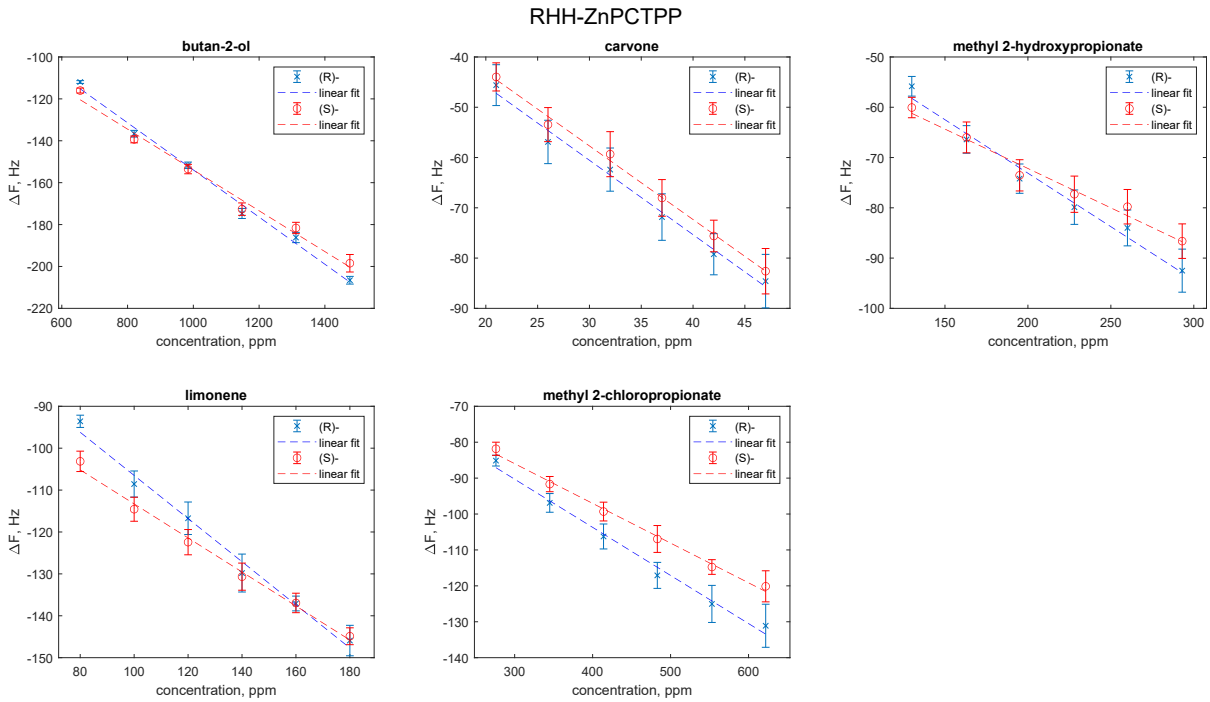

Figure S10. Characteristic curves of RHH-ZnpCTPP sensor to the five enantiomer pairs.

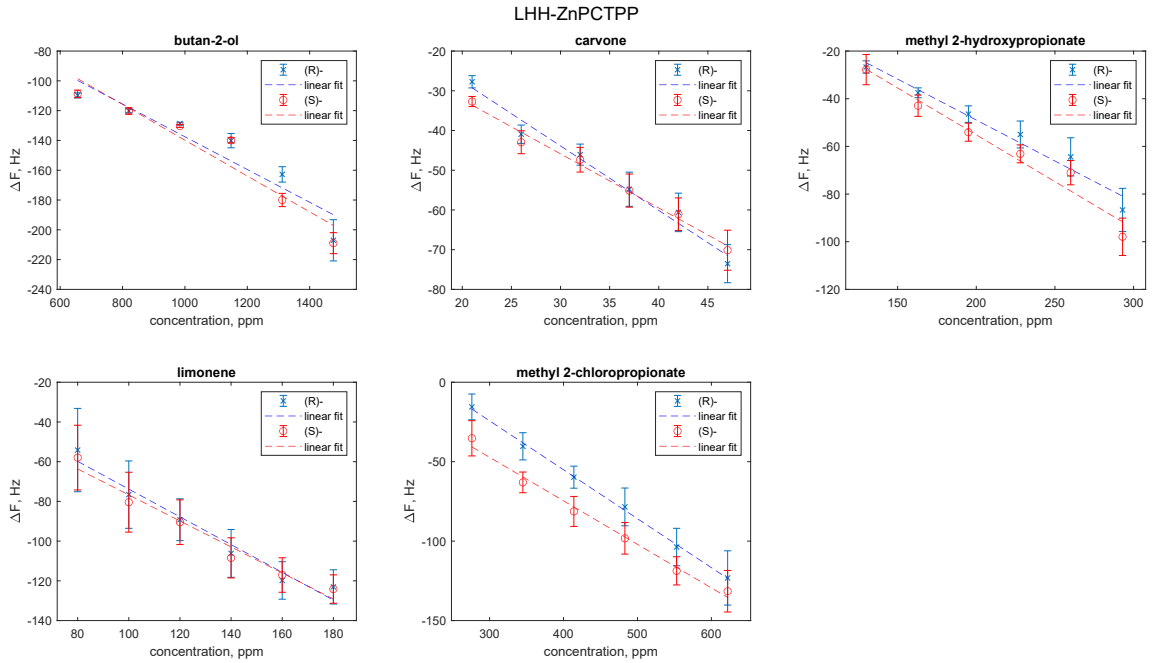

Figure S11. Characteristic curves of LHH-ZnpCTPP sensor to the five enantiomer pairs.

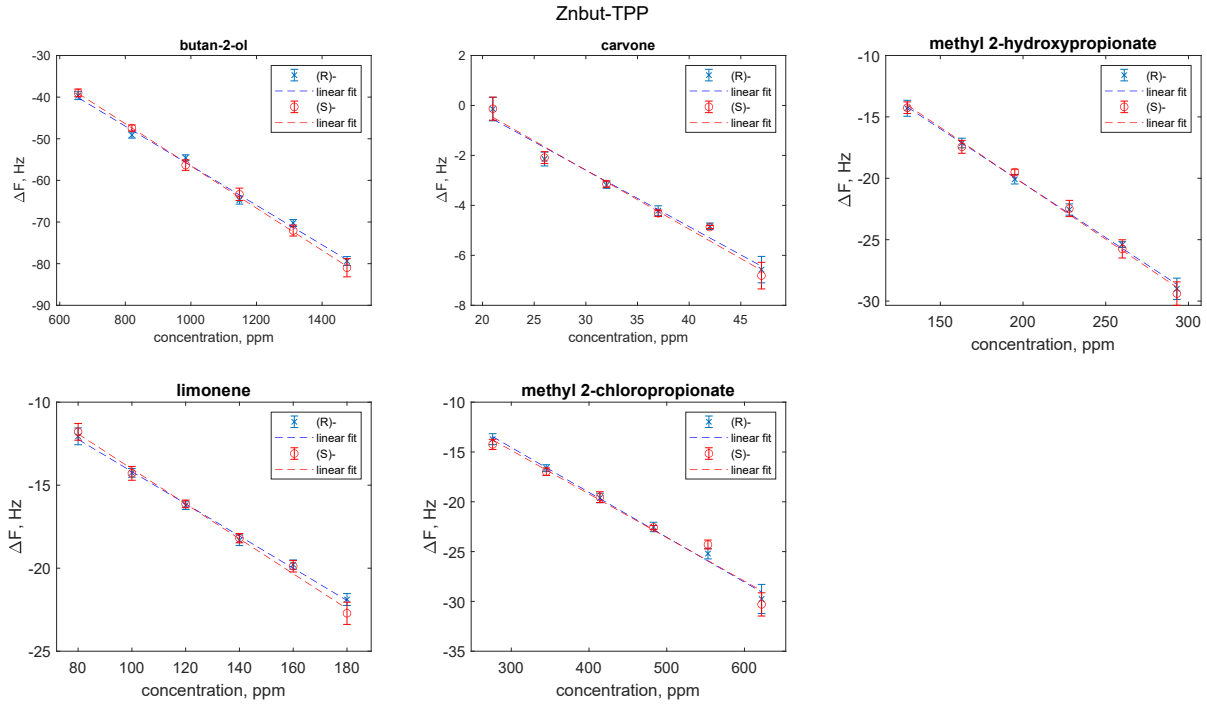

Figure S12. Characteristic curves of Znbut-TPP sensor to the five enantiomer pairs. We utilized this sensor as the achiral element.

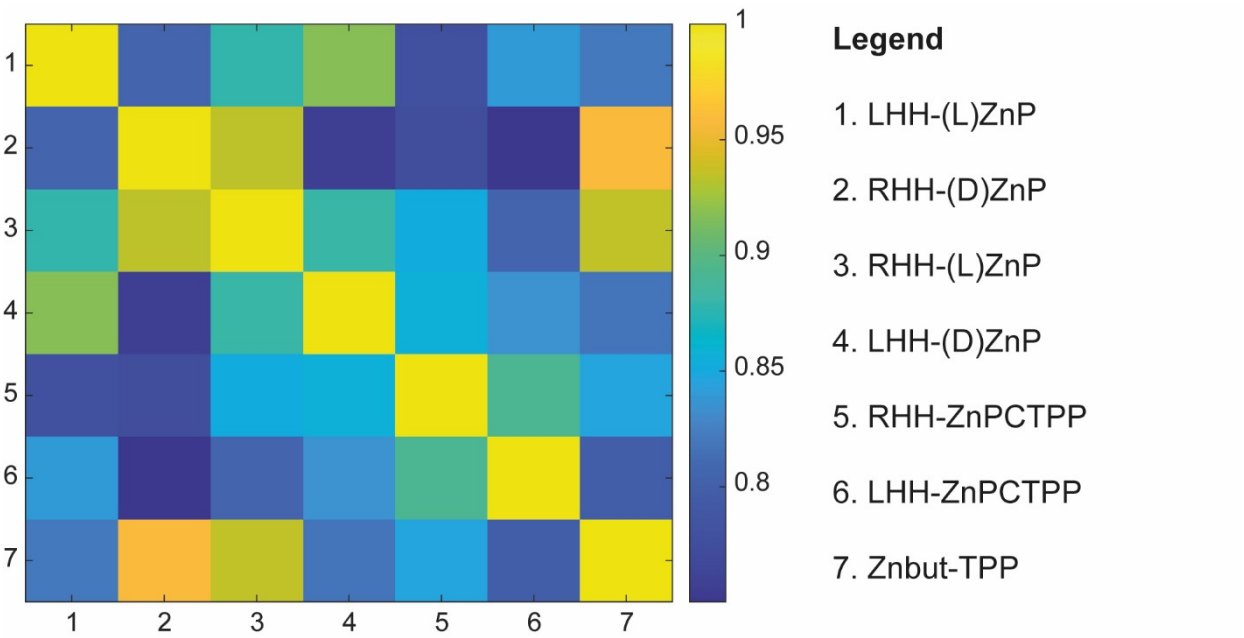

Figure S13. Pearson correlation matrix considering all sensor responses.

Table S3. Average response time for each sensor. S1=LHH-(L)ZnP; S2=RHH-(D)ZnP; S3=RHH-(L)ZnP; S4=LHH-(D)ZnP; S5=RHH-ZnpCTPP; S6=LHH-ZnpCTPP; S7=Znbut-TPP.

	T90 (s)													
	S1		**S2**		**S3**		**S4**		**S5**		**S6**		**S7**	
	R	**S**	**R**	**S**	**R**	**S**	**R**	**S**	**R**	**S**	**R**	**S**	**R**	**S**
butan-2-ol	84	81	81	80	87	85	91	89	65	64	110	110	78	78
carvone	100	95	102	99	97	95	106	110	83	84	104	102	118	114
methyl 2-hydroxypropionate	84	88	88	85	114	109	96	106	81	86	87	69	84	89
limonene	58	59	54	57	56	52	91	88	77	73	91	85	59	63
methyl 2-chloropropionate	57	52	68	62	67	62	99	94	65	72	84	71	73	71

4.2 Features extraction

The features extracted from the adsorption phase are 6; in the same way, these from the desorption phase are 5; in total, they are 11 for each sensor. Frequency shifts (DF, DF75, DF50, DF25, DF10, and DF05) were measured at T, ¾T, T/2, T/4, T/10, and T/20, respectively. Since recovery is always complete, DF100 during the desorption coincides with DF during adsorption and has been removed.

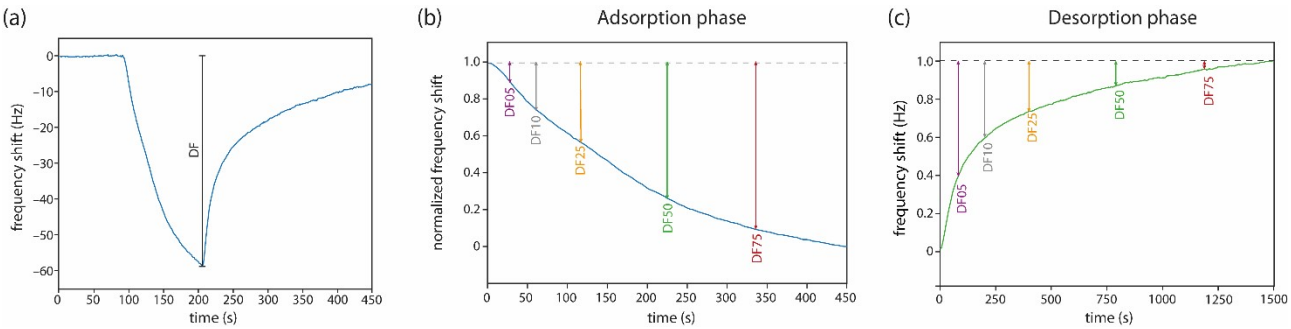

Figure S14. Schematic representation of features extracted from sensors. Similar features have been extracted from the desorption phase.

4.2 Multivariate analysis

4.2.1 Principal Component Analysis (PCA)

A simple method to analyse array properties is Principal Component Analysis (PCA). Sensor response is represented in an n-dimensional vector space, where "n" corresponds to the number of features extracted from sensors that constitute the array. In other words, each descriptor defines an axis of the space. A correlation exists between features describing sensor data if the sensors are not specific or are broadly selective. PCA is a simple algorithm to remove correlation by defining a new

set of orthogonal bases obtained as a linear combination of sensor responses. These new uncorrelated variables are called Principal Components.

Furthermore, PCA orders the new features according to the amount of variance expressed. The first principal component contains a high percentage of variance, as expected for datasets containing analytes measured at different concentrations. Sensor responses are proportional to the concentration, whose information dominates the first principal component due to the extensive range of concentrations tested. As expected by the complexity of the task, the separation between enantiomers of the same compounds is not captured in the first principal components for all the compounds. Still, it is necessary to consider the minor order Principal Component to obtain a full separation between all the classes.

In our case, the data matrix is composed of 420 samples expressed by 77 features. Data have been autoscaled before performing PCA. Autoscaling transforms each feature in an adimensional descriptor in which data distribution has null mean and unitary variance by the formula:

$$z = \frac{x - \mu}{\sigma}$$

4.2.2 Confusion matrix

Results are summarized using the confusion matrices. In particular, the confusion matrix represents a simple method to evaluate the classifier performances: the columns contain predicted classes, and the rows contain actual classes. The element (i,j) reports all cases in which the model has classified the actual class i as class j. For the sake of clarity, we decided to show the classification percentage for each element (i,j): each value has been calculated as the ratio between the element (i,j) and the sum of the element on row i (the same class), multiplied by 100. The confusion matrix shows immediately if the classifier confuses the classes with each other. All the elements on the matrix diagonal are classified correctly, while the others are classified incorrectly.

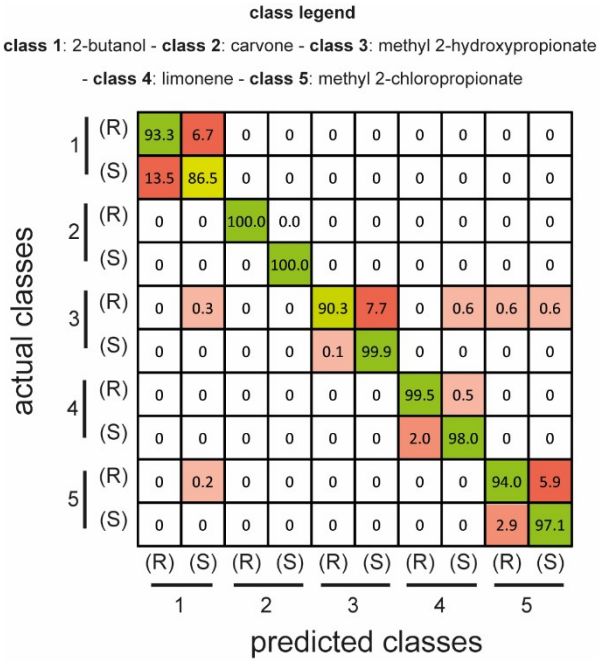

Figure S15. The confusion matrix obtained from the classification model that is trained on samples belonging only to three random concentrations and validate on the remaining concentrations. The LDA model has been trained considering 10 classes.

References ,

1. P. Liu, Y. Battie, Y. Okazaki, N. Ryu, E. Pouget, S. Nlate, T. Sagawa and R. Oda, *Chem. Commun.,* 2021, 57, 12024.
2. N. Ryu, Y. Okazaki, K. Hirai, M. Takafuji, S. Nagaoka, E. Pouget, H. Ihara and R. Oda, *Chem. Commun.,* 2016, 52, 5800.
3. Y. Okazaki, N. Ryu, T. Buffeteau, S. Pathan, S. Nagaoka, E. Pouget, S. Nlate, H. Ihara and R. Oda, *Chem. Commun.*, 2018, 54, 10244.
4. T. Delclos, C. Aimé, E. Pouget, A. Brizard, I. Huc, M. H. Delville and R.Oda, *Nano Lett.*, 2008, 8, 1929.
5. P. Liu, W. Chen, Y. Okazaki, Y. Battie, L. Brocard, M. Decossas, E. Pouget, P. Müller-Buschbaum, B. Kauffmann, S. Pathan, T. Sagawa and R. Oda, *Nano Lett.*, 2020, 20, DOI:10.1021/acs.nanolett.0c02013.